PAPER

Check for updates

Theoretical investigation of the excited-state intramolecular double proton transfer process of 2,2′-(benzo[1,2-d:4,5-d′]bis(thiazole)-2,6-diyl) diphenol†

Yongchao Hao, [iD] *[ab] Xiaoran Li,[a] Hongfang Li,[a] Shanyan Chang,[a] Jiangyu Zhang[a] and Lili Dong*[a]

In this work, the excited state intramolecular double proton transfer (ESIDPT) mechanism of 2,2′-(benzo[1,2-d:4,5-d′]bis(thiazole)-2,6-diyl)diphenol (**BTAP**) is proposed using density functional theory (DFT) and time-dependent DFT (TDDFT). The changes in bond lengths, bond angles and IR vibrational spectra associated with two intramolecular hydrogen bonds of **BTAP** upon photoexcitation indicate that the hydrogen bonds are strengthened in the excited state, facilitating the ESIDPT process. Investigation of the constructed S_1-state potential energy surface proposes that **BTAP** prefers a stepwise ESIDPT mechanism. Electronic spectra and frontier molecular orbitals (FMOs) are also presented to illustrate the luminescent properties of **BTAP**.

1. Introduction

Proton transfer is one of the fundamental processes in the fields of chemistry, biology and physics. Since Weller discovered the dual-emission property in salicylic acid and attributed the large Stokes-shifted fluorescent emission to the excited state intramolecular proton transfer (ESIPT) mechanism, the ESIPT process has been elaborated systematically using experimental and theoretical methods.[1–12] It is widely accepted that the ESIPT process occurs *via* a four-step photophysical scheme: (1) transition to the excited state upon photoexcitation, (2) proton transfer with an intramolecular hydrogen bond to form a phototautomer, (3) radiative relaxation to produce a large Stokes-shifted fluorescence to the ground state, and (4) reverse proton transfer. Owing to the unique feature of ESIPT, this mechanism has been applied to the design of fluorescent probes,[13–19] bio-imaging techniques,[20–26] white-light OLEDs[27–30] and so on.

Biological systems typically involve two or more proton transfers, whereas most excited state intramolecular proton transfer processes involve only a single proton transfer. In order to mimic the proton relay in biochemical processes, there is an urgent need to design and investigate molecular models with excited state double or multiple proton transfer properties. In recent years, excited-state intramolecular double proton transfer (ESIDPT) has gradually received widespread attention. G. Krishnamoorthy *et al.*[31] performed a comprehensive experimental and theoretical analysis on the ESIDPT characteristics of a fluorescent molecule, 2,2′-(1,4-phenylenebis(1H-benzo[d]imidazole-1,2-diyl))diphenol, which contained two 2-(2′-hydroxyphenyl)benzimidazole unit. Zhao *et al.*[32] presented 2,5-bis(4,5-diphenyl-1H-imidazole-2-yl)benzene-1,4-diol derivatives bearing double intramolecular hydrogen bonds and further elucidated the effects of chalcogen substitution on hydrogen bond interactions and the ESIPT mechanism. Yongqing Li and co-workers[33] confirmed a stepwise ESIDPT mechanism of 2,2′-bipyridine-3,3′-diol-5,5′-dicarboxylic acid ethyl ester and proposed a method to regulate the stepwise ESIDPT process through solvent polarity and external electric field. Apart from these examples, some different types of ESIDPT compounds have been reported;[34–42] however, the number of ESIDPT model molecules is still limited.

In this work, we theoretically investigated the ESIDPT mechanism of a new model molecule 2,2′-(benzo[1,2-d:4,5-d′]bis(thiazole)-2,6-diyl)diphenol (**BTAP**), which bears the phenol group as the hydrogen bond donor and benzobisthiazole group as the hydrogen bond acceptor. The geometric structures of **BTAP** and its ESIPT isomers in the ground and excited states are optimized using density-functional theory (DFT) and time-dependent density-functional theory (TDDFT), as shown in Fig. 1. The bond lengths, bond angles and infrared vibration spectrum related to intramolecular hydrogen bonds are analyzed in detail to reveal the effect of photoexcitation on intramolecular hydrogen bonds. The potential energy surfaces

[a]*School of Chemical Engineering and Biotechnology, Xingtai University, Xingtai 054001, China. E-mail: 201610338@xttc.edu.cn; donglilihanzh@163.com*

[b]*College of Chemistry and Materials Science, Hebei Normal University, Shijiazhuang 050024, China*
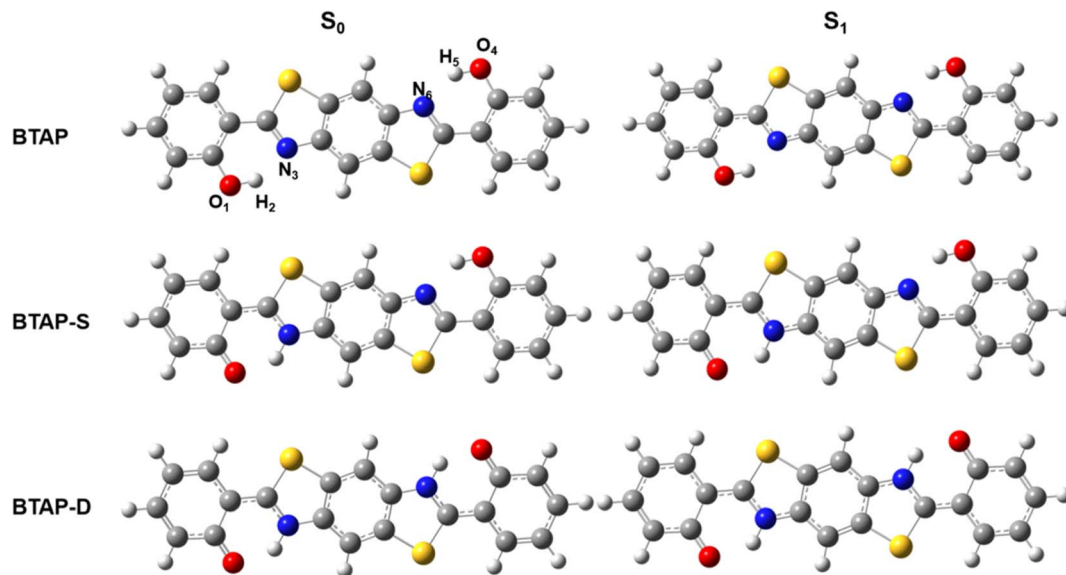
Fig. 1 Optimized geometry structures of BTAP, its single proton transfer tautomer BTAP-S and double proton transfer tautomer BTAP-D.

in the S_0 and S_1 states are constructed to elaborate the ESIDPT mechanism of **BTAP**. We also provide electronic spectra and frontier molecular orbitals (FMOs) to illustrate the luminescent properties of **BTAP**.

2. Computational details

All theoretical calculations presented were carried out using Gaussian 09 software.[43] Geometry optimizations of the ground state and excited state were performed *via* density functional theory (DFT) and time-depend density functional theory (TDDFT) methods, respectively, using Becke's three-parameter hybrid exchange functional with the Lee–Yang–Parr gradient-corrected correlation functional (B3LYP)[44,45] and 6-31++G(d, p) basis set. The incorporation of Grimme's D3 version of dispersion in all calculations ensures the comprehensive consideration of the dispersion forces. To be consistent with the experimental result, dichloromethane was used as the solvent with the polarizable continuum model (PCM) with the integral equation formalism variant (IEFPCM).[46] The geometry optimizations were performed without constraints on bond lengths, angles, or dihedral angles. All the local minima were determined without the imaginary modes by vibrational analysis calculations. Based on the optimized structures, the absorption and fluorescent spectra were calculated at the B3LYP/6-31++G(d, p) level. In addition, to study the proton transfer behavior of the molecule, the potential energy surface surfaces (PESs) were scanned at S_0 and S_1 states by gradually extending the bond lengths of O_1–H_2 and O_4–H_5, respectively, without structural constraints.

3. Results and discussion

3.1. Geometry structure and hydrogen bond

Geometry optimization of the ESIPT isomers of **BTAP** molecule in S_0 and S_1 states was conducted using the B3LYP functional

and 6-31++G(d, p) basis set. The optimized ESIPT isomer structures of **BTAP**, **BTAP-S** (single proton transfer form) and **BTAP-D** (double proton transfer form) in the S_0 and S_1 states are shown in Fig. 1. Since photoexcited ESIPT behaviors are closely related to intramolecular double hydrogen bonding interactions, the effects of photoexcitation on hydrogen bonding effects were elaborated first. All atoms involved in intramolecular hydrogen bonding were numbered as O_1–H_2⋯N_3 and O_4–H_5⋯N_6 for description. Considering the symmetry of the molecular structure, the structural changes on both sides of the molecule were consistent.

The change of hydrogen bond strength before and after photo-excitation was illustrated by comparing the bond lengths, bond angles and vibrational frequency of intramolecular hydrogen bonds in ground and excited states. Some important structural parameters associated with hydrogen bonds are shown in Table 1. For the **BTAP** form, the bond lengths of O_1–H_2 and O_4–H_5 were elongated from 0.995 Å (S_0) to 1.000 Å (S_1). The hydrogen bond lengths of H_2⋯N_3 and H_5⋯N_6 are shortened from 1.758 Å (S_0) to 1.739 Å (S_1), which indicated that the intramolecular hydrogen bond in the S_1 state was strengthened. The increase in the bond angles of O_1–H_2⋯N_3 and O_4–H_5⋯N_6 from 146.0° to 147.0° confirmed the enhancement of hydrogen

Table 1 The primary bond lengths (Å) and bond angles δ (°) of BTAP, BTAP-S and BTAP-D structures in the S_0 and S_1 states

	BTAP		BTAP-S		BTAP-D	
	S_0	S_1	S_0	S_1	S_0	S_1
O_1–H_2	0.995	1.000	0.994	0.995	1.676	1.763
H_2–N_3	1.758	1.739	1.763	1.754	1.049	1.039
O_4–H_5	0.995	1.000	1.680	1.836	1.676	1.763
H_5–N_6	1.758	1.739	1.049	1.032	1.049	1.039
$\delta(O_1$–H_2–$N_3)$	146.0°	147.0°	145.9°	146.8°	137.8°	135.0°
$\delta(O_4$–H_5–$N_6)$	146.0°	147.0°	137.3°	132.6°	137.8°	135.0°

bonds in the S_1 state. For the **BTAP-S** form, compared with the S_0 state, the bond length of hydroxyl (O_4–H_5) is lengthened, the distance of hydrogen bond (H_5···N_6) is shortened, and the bond angle (O_4–H_5···N_6) of the hydrogen bond is enlarged in the S_1 state. The changes in bond length and angle of the **BTAP** and **BTAP-S** indicate that the intramolecular hydrogen bonds of enol segment tautomers are enhanced in the S_1 state, meaning that the ESIPT reaction is more likely to occur in the S_1 state. In contrast, the structural changes of keto's segments in **BTAP-S** (O_1–H_2···N_3) and **BTAP-D** (O_1–H_2···N_3 and O_4–H_5···N_6) show that the intramolecular hydrogen bonds are weakened in the S_1 state, indicating that the reverse ESIPT prefer to occur in the S_0 state.

The infrared vibration spectra analysis at the hydrogen bond sites is also used to elaborate on the changes in the hydrogen bond strength between the ground state and the excited state. Herein, the theoretical IR results involved in stretching vibration of hydrogen bond sites in **BTAP**, **BTAP-S** and **BTAP-D** are presented in Fig. 2. As shown in Fig. 2, the vibration frequencies of O_1–H_2 (O_4–H_5) for **BTAP** are located at 3251 cm^{-1} in the S_0 state and turn to 3152 cm^{-1} after photoexcitation to the S_1 state. The vibration frequencies are red-shifted by 99 cm^{-1} when **BTAP** is photoexcited from the S_0 state to the S_1 state. It means that hydrogen bonds are enhanced, facilitating the process of intramolecular proton transfer in the excited state. For the **BTAP-S** form, the vibration frequency of O_4–H_5 is red-shifted by 34 cm^{-1} from 3264 cm^{-1} in the S_0 state to 3230 cm^{-1} in the S_1 state, which indicates that the hydrogen bond O_4–H_5···N_6 is enhanced in the S_1 state. However, the blue-shift of 288 cm^{-1} occurs for H_2–N_3 from 3017 cm^{-1} in the S_0 state to 3305 cm^{-1} in the S_1 state, and the hydrogen bond strength O_1–H_2···N_3 is superior in the S_0 state than in the S_1 state. Similarly, the stretch vibrational frequency of N_3–H_2 (N_6–H_5) in **BTAP-D** is also blue-shifted by 179 cm^{-1} from 3004 cm^{-1} in the S_0 state to 3183 cm^{-1} in the S_1 state, which illustrates that the intensity of the hydrogen bond O_1–H_2···N_3 (O_4–H_5···N_6) is stronger in the S_0

state than in the S_1 state. In summary, the infrared vibration analysis indicates that the proton transfer process is more likely to occur in the excited state while the inverse proton transfer process is more likely to occur in the ground state, which is consistent with the analysis of changes in geometry structure parameters.

3.2. Potential energy surfaces and proton transfer process

To illustrate the ESIPT mechanism further and to explore whether the double proton transfer occurs stepwise or synchronously, and the calculations of potential energy surfaces (PESs) were performed using the constrained optimizations in the S_0 state and S_1 state geometrical structures of **BTAP** along with the fixed O_1–H_2 bond length and O_4–H_5 bond length. As shown in Fig. 3, the PESs of the S_0 state is scanned with varying the O_1–H_2 and O_4–H_5 bond lengths from 0.995 to 2.15 Å in steps of 0.05 Å. There exist four local minimum points whose coordinates are located at A (1.00 Å, 1.00 Å), B (1.00 Å, 1.70 Å), C (1.70 Å, 1.00 Å) and D (1.70 Å, 1.70 Å). Owing to the symmetry of the molecular structure, point B and point C exhibit significant symmetrical characteristics and the energy values of the two points are equal. It is not difficult to find that points A, B (C) and D can approximatively represent **BTAP**, **BTAP-S** and **BTAP-D**, respectively. The calculated results show that the energies of the four local minimum points from large to small are $E_D > E_C = E_B > E_A$ in the S_0 state. Thus, the **BTAP** prefers to exist in the form of an enol tautomer in the S_0 state. Similarly, there also exist four stable points on the potential energy surface of the S_1 state, whose coordinates located A* (1.00 Å, 1.00 Å), B* (1.00 Å, 1.80 Å), C* (1.80 Å, 1.00 Å) and D* (1.75 Å, 1.75 Å). The potential energy barriers among these stable configurations of the S_0 and S_1 states are also listed in Table 2. As shown in Table 2, the potential energy barriers in the S_1 state are relatively lower than those in the S_0 state, indicating that the proton transfer process is easier to occur in the S_1 state than in the S_0 state. The synchronous double proton transfer (**BTAP** → **BTAP-D**) and the sequential single proton transfer (**BTAP** → **BTAP-S** → **BTAP-D**) are the two primary pathways for the excited state intramolecular double proton transfer of **BTAP**. The potential energy barrier of the pathway (**BTAP** → **BTAP-D**) is 17.8 kcal mol^{-1} and is too high to overcome the energy barrier, hence the double proton transfer is difficult to happen spontaneously. However, the acceptable barrier of 7.9 kcal mol^{-1} (**BTAP** → **BTAP-S**) implies the possibility of proton transfer, leading to the generation of **BTAP-S**. Subsequently, another proton would transfer to form **BTAP-D** across a mild barrier of 11.4 kcal mol^{-1} (**BTAP-S** → **BTAP-D**). Therefore, it is very likely that the double proton transfer undergoes a stepwise mechanism. Because the energies of the four local minimum points from large to small follow $E_{D*} > E_{A*} > E_{C*} = E_{B*}$ in the S_1 state, the energy barrier of the reverse proton transfer process for **BTAP-D** → **BTAP-S** (2 kcal mol^{-1}) is lower than the one of the forward proton transfer process and **BTAP-S** → **BTAP** (8.1 kcal mol^{-1}) is very close to the one of the forward proton transfer process, suggesting that the proton transfer process is reversible and the tautomers **BTAP**, **BTAP-S**, and **BTAP-D** coexist in the S_1 state.
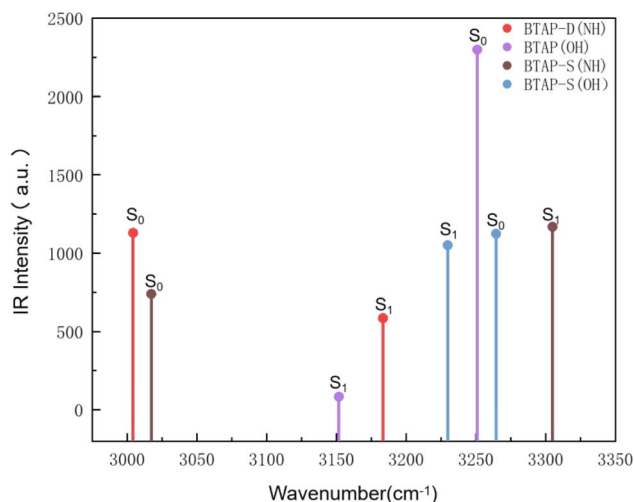

Fig. 2 Calculated infrared vibration spectra of BTAP, BTAP-S and BTAP-D in the spectral region of OH and NH stretching bands in S_0 and S_1 states.
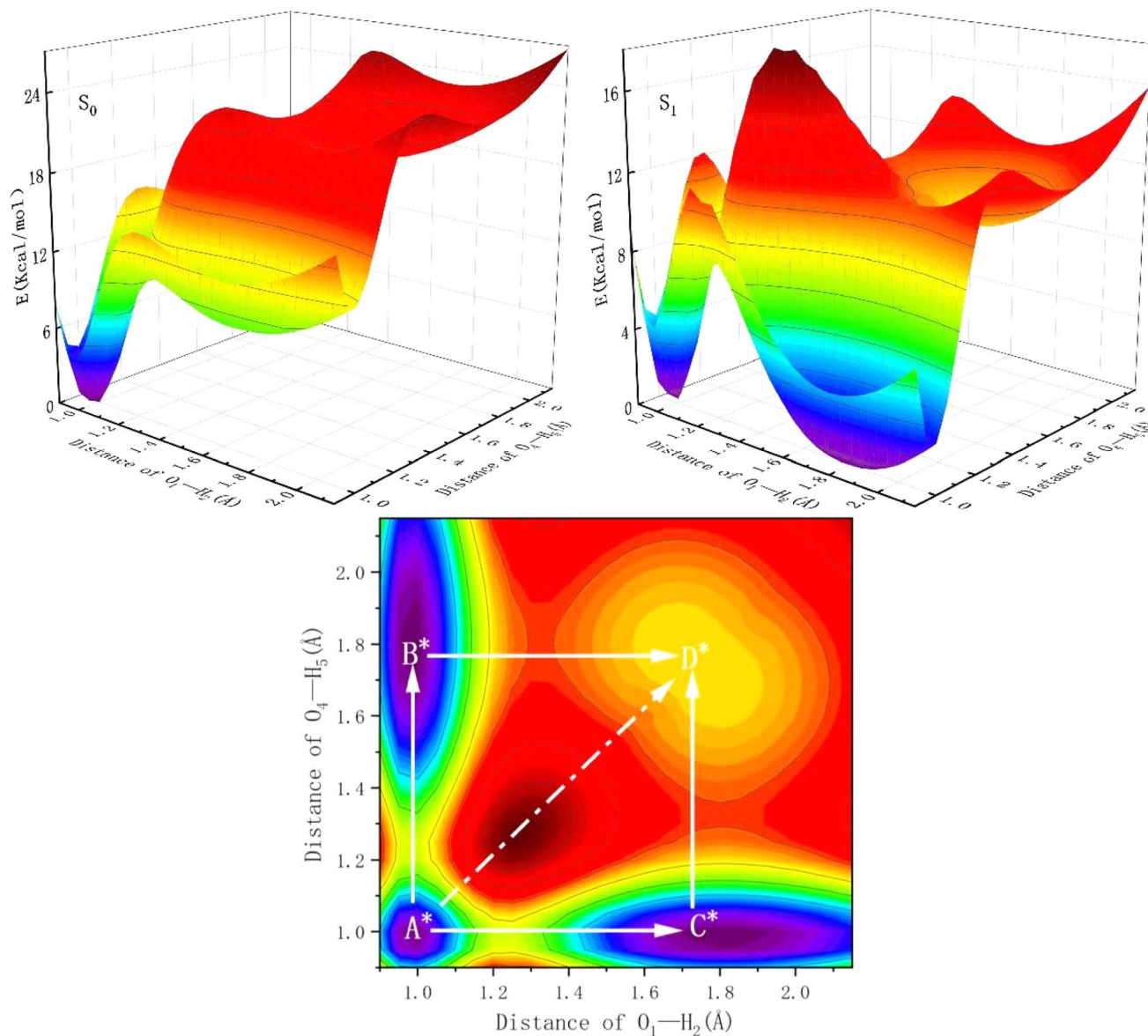
Fig. 3 The potential energy surfaces of the **BTAP** system in the S_0 and S_1 states and the projective plane in the S_1 state as functions of O_1–H_2 and O_4–H_5 bond lengths.

Table 2 The potential energy barriers (kcal mol^{-1}) in S_0 and S_1 states (E': reverse processes)

	$E_{A \to B}$	$E_{B \to D}$	$E_{A \to D}$	$E_{A^* \to B^*}$	$E_{B^* \to D^*}$	$E_{A^* \to D^*}$
E	11.2	11.5	22.6	7.9	11.4	17.8
E'	1.9	1.8	3.6	8.1	2	8.6

3.3. Electronic spectra and frontier molecular orbitals

As the result of PESs shows, there exist three tautomers **BTAP**, **BTAP-S**, and **BTAP-D** in the S_1 state, which would emit fluorescence upon photo-excitation. Therefore, the absorption and fluorescence spectra of the three molecules are simulated at the B3LYP/6-31++G(d, p) level. The absorption spectrum is shown in Fig. 4. The computational absorption peak value of **BTAP** in dichloromethane is 388 nm and coincides well with the experimental value of 386 nm (Fig. S1†). In addition, the fluorescence spectra in dichloromethane are shown in Fig. 4. The calculated fluorescence peak values of **BTAP**, **BTAP-S** and **BTAP-D** are 442 nm, 518 nm and 527 nm, respectively. The normal emission of **BTAP** with a Stokes shift of 57 nm is in good agreement with the experimental value of 403 nm. The two fluorescent emission peaks of **BTAP-S** and **BTAP-D** are very close and overlap to form one peak so that only one large stokes-shifted fluorescent emission peak of keto-forms at 523 nm appears in the experimental spectrum. The perfect agreement of the spectral data demonstrates the rationality of the simulation using the DFT/TD-DFT methods with B3LYP functional and 6-31++G(d, p) basis set.

The charge distribution and charge transfer induced by photo-excitation can depict qualitatively the properties of the
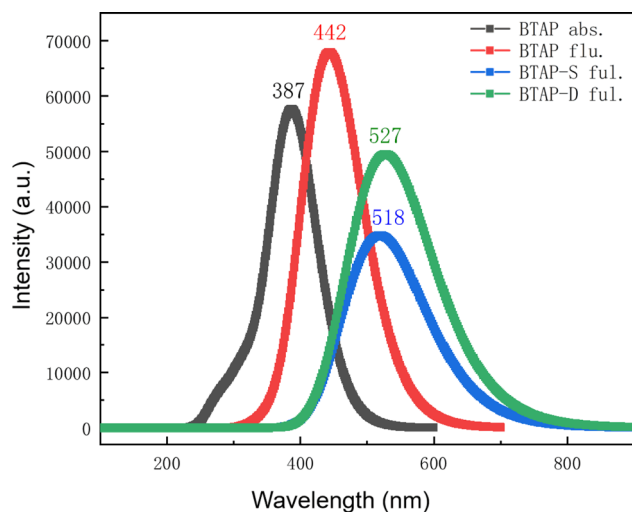
Fig. 4 Theoretical electronic spectra of **BTAP**, **BTAP-S** and **BTAP-D** in DCM.

Table 3 The Mulliken's charge of O_1, H_2, N_3, O_4, H_5 and N_6 atoms for BTAP in both S_0 and S_1 states

Atoms	S_0	S_1
O_1	−0.679	−0.670
H_2	0.560	0.560
N_3	−0.253	−0.251
O_4	−0.679	−0.670
H_5	0.560	0.560
N_6	−0.253	−0.251

excited state and frontier molecular orbitals (FMOs) mainly contributing to the S_0–S_1 transition, hence, the frontier MOs of **BTAP** are analyzed in dichloromethane solvent to explore the nature of the excited state. The highest occupied molecular orbital (HOMO) and lowest unoccupied molecular orbital (LUMO) orbital are calculated and shown in Fig. 5. Both HOMO and LUMO orbitals exhibit a π character, showing that the $S_0 \rightarrow S_1$ transition is an allowed $\pi\pi$*-type transition. Mulliken's charge analysis is adopted for a detailed investigation of the charge distribution over the atoms involved in intramolecular hydrogen bonds and is used to explore the influence of charge transfer on the excited state proton transfer process. As shown in Table 3, the electron density on the O atom and N atom decreases from the S_0 state to the S_1 state, and it decreases more on the O atom for the BTAP tautomer. The negative charge of the O_1 atom (O_4 atom) decreases from −0.679 in the S_0 state to −0.670 in the S_1 state, meanwhile, a slight decrease from −0.253 to −0.251 in the negative charge of the N_4 atom (N_5 atom) occurs. This evidence indicates that the intensity of the hydroxyl group weakens and the intensity of the hydrogen bond strengthens in the S_1 state for **BTAP**, which facilitates the ESIPT reaction.
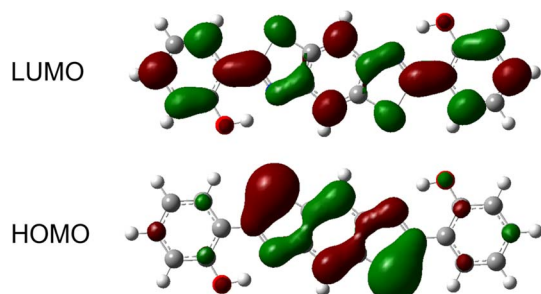
4. Conclusions

In this work, the ESIPT mechanism of 2,2′-(benzo[1,2-*d*:4,5-*d′*] bis(thiazole)-2,6-diyl)diphenol was systematically investigated based on the DFT/TD-DFT methods. By comparing the changes in bond length, bond angle, and infrared vibration spectrum between the ground state and excited state, we observed a significant enhancement of the intramolecular hydrogen bond in the excited state, which promotes the occurrence of proton transfer reactions. The scanned PESs show that the potential energy barrier of the synchronous double proton transfer is so high that the two protons cannot transfer simultaneously in the excited state, therefore, the **BTAP** follows a stepwise ESIPT process which has a lower barrier that is easily overcome. The spectral data obtained from theoretical calculations is consistent with the experimental ones, validating the rationality of the theoretical simulation methods used in this work. The FMOs and Mulliken's charge analysis exhibit that the charge transfer upon photoexcitation enhances the proton transfer process.

Data availability

The data supporting this article have been included within the manuscript and its ESI.†

Author contributions

Yongchao Hao: Writing – original draft; theoretical calculation; methodology; funding acquisition; resources; supervision. Xiaoran Li: data curation; formal analysis. Hongfang Li: data curation. Shanyan Chang: data curation. Jiangyu Zhang: formal analysis; Lili Dong: funding acquisition; resources; supervision.

Conflicts of interest

There are no conflicts to declare.

Acknowledgements

Fig. 5 Frontier molecular orbitals (HOMO and LUMO) of the **BTAP** form.

References

1 H. Gu, W. J. Wang, W. Y. Wu, M. L. Wang, Y. R. Liu, Y. J. Jiao, F. Wang, F. Wang and X. Q. Chen, *Chem. Commun.*, 2023, **59**, 2056–2071.

2 J. F. Zhao, P. Song, L. Feng, X. Wang and Z. Tang, *J. Mol. Liq.*, 2023, **380**, 121763.

3 O. Anitha, M. Mathivanan, B. Tharmalingam, T. Thiruppathiraja, S. Ghorai, R. Natarajan, V. Thiagarajan, S. Lakshmipathi and B. Murugesapandian, *Dyes Pigments*, 2023, **212**, 111091.

4 K. Liu, J. Zhang, Q. Y. Shi, L. P. Ding, T. H. Liu and Y. Fang, *J. Am. Chem. Soc.*, 2023, **145**, 7408–7415.

5 T. Frizon, C. Salla, F. Grillo, F. S. Rodembusch, V. S. Câmara, H. C. Silva, E. Zapp, E. Junca, F. Z. Galetto, A. M. de Costa, G. J. Pedroso, A. A. Chepluki, S. Saba and J. Rafique, *Spectrochim. Acta, Part A*, 2023, **288**, 122050.

6 J. F. Zhao, B. Jin and Z. Tang, *Phys. Chem. Chem. Phys.*, 2022, **24**, 27660–27669.

7 S. Kaya, H. G. Aydin, S. Keskin, Z. Ekmekci and N. Menges, *J. Photochem. Photobiol., A*, 2021, **420**, 113487.

8 S. Ding, A. X. Xu, A. K. Sun, Y. Xia and Y. J. Liu, *Spectrochim. Acta, Part A*, 2021, **245**, 118937.

9 Y. T. Qi, Z. Tang, H. B. Zhan, Y. Wang, Y. L. Zhao, X. Fei, J. Tian, L. Yu and J. Y. Liu, *Spectrochim. Acta, Part A*, 2020, **224**, 117359.

10 B. Kuzu, M. Tan, Z. Ekmekci and N. Menges, *J. Photochem. Photobiol., A*, 2019, **381**, 111874.

11 S. Y. Yin, S. S. Sun, M. Pan, L. Chen, Z. Wang, Y. J. Hou, Y. N. Fan, H. P. Wang and C. Y. Su, *J. Photochem. Photobiol., A*, 2018, **355**, 377–381.

12 N. Suzuki, A. Fukazawa, K. Nagura, S. Saito, H. Kitoh-Nishioka, D. Yokogawa, S. Irle and S. Yamaguchi, *Angew. Chem. Int. Ed.*, 2014, **53**, 8231–8235.

13 A. I. Said, N. I. Georgiev and V. B. Bojinov, *J. Photochem. Photobiol., A*, 2024, **446**, 115176.

14 Y. R. Huang, Y. Li, Y. Li, K. L. Zhong and L. J. Tang, *New J. Chem.*, 2023, **47**, 6916–6923.

15 H. X. Ren, F. J. Huo, W. Wen and C. X. Yin, *Dyes Pigments*, 2022, **199**, 110111.

16 A. Y. Bi, M. Liu, S. Huang, F. Zheng, J. P. Ding, J. Y. Wu, G. Tang and W. B. Zeng, *Chem. Commun.*, 2021, **57**, 3496–3499.

17 N. Nehra, R. Kaushik, D. G. Vikas and R. K. Tittal, *J. Mol. Struct.*, 2020, **1207**, 127839.

18 X. X. Tang, X. G. Zhu, H. L. Xu, H. Sun, X. Han, Q. Li, B. B. Zhou and Z. H. Ni, *Spectrochim. Acta, Part A*, 2022, **281**, 121567.

19 H. N. Peng, X. M. Peng, J. Q. Huang, A. Huang, S. J. Xu, J. J. Zhou, S. S. Huang and X. P. Cai, *J. Mol. Struct.*, 2020, **1212**, 128138.

20 T. X. Xiao, C. Bao, L. L. Zhang, K. Diao, D. X. Ren, C. X. Wei, Z. Y. Li and X. Q. Sun, *J. Mater. Chem. A*, 2022, **10**, 8528–8534.

21 S. Bhowal and A. Ghosh, *RSC Adv.*, 2021, **11**, 27787–27800.

22 H. Y. Xu, W. Chen, L. X. Ju and H. F. Lu, *Spectrochim. Acta, Part A*, 2021, **247**, 119074.

23 D. Aydin, I. B. Gunay, S. Elmas, T. Savran, F. N. Arslan, G. Sadi and I. Yilmaz, *New J. Chem.*, 2020, **44**, 12079–12089.

24 P. Zhang, Y. Z. Xiao, Q. Zhang, Z. X. Zhang, H. W. Yu and C. F. Ding, *New J. Chem.*, 2019, **43**, 7620–7627.

25 C. Balakrishnan, M. A. Neelakantan and S. Banerjee, *Sens. Actuators, B*, 2017, **253**, 1012–1025.

26 R. Alam, T. Mistri, R. Bhowmick, A. Katarkar, K. Chaudhuri and M. Ali, *RSC Adv.*, 2016, **6**, 1268–1278.

27 L. Duarte, J. C. Germino, J. F. Berbigier, C. A. Barboza, M. M. Faleiros, D. D. Simoni, M. T. Galante, M. S. de Holanda, F. S. Rodembusch and T. Atvars, *Phys. Chem. Chem. Phys.*, 2019, **21**, 1172–1182.

28 L. Duarte, J. C. Germino, R. A. Mendes, J. F. Berbigier, M. M. Faleiros, F. S. Rodembusch and T. Atvars, *Dyes Pigments*, 2019, **171**, 107671.

29 M. Mohan, M. N. Satyanarayan and D. R. Trivedi, *New J. Chem.*, 2019, **43**, 10413–10428.

30 W. J. Yang and X. B. Chen, *Phys. Chem. Chem. Phys.*, 2014, **16**, 4242–4250.

31 A. Das Kanungo, Ila, S. Panda, U. Phukon, M. Sathiyendran and G. Krishnamoorthy, *J. Photochem. Photobiol., A*, 2024, **450**, 115412.

32 C. Liu, J. Zhao, J. Chen, M. Wang, M. Hou and L. Yang, *Phys. Chem. Chem. Phys.*, 2024, **26**, 6335–6344.

33 H. Zhuang, W. Shi, G. Zhao and Y. Li, *Phys. Chem. Chem. Phys.*, 2024, **26**, 12016–12026.

34 X. Tang, Y. Zhang and C. Sun, *Phys. Chem. Chem. Phys.*, 2024, **26**, 10439–10448.

35 J. Zhao and C. Liu, *Molecules*, 2023, **28**, 5951.

36 J. Zhao, H. Zhang, L. Fan, F. Li and P. Song, *Spectrochim. Acta, Part A*, 2023, **299**, 122831.

37 X. Xin, W. Shi, Y. Zhao, G. Zhao and Y. Li, *Chem. Phys.*, 2023, **570**, 111882.

38 D. Ushakou, *J. Lumin.*, 2023, **263**, 120032.

39 H. Mu, D. Li, J. Gao, Y. Wang, Y. Zhang, G. Jin and H. Li, *J. Mol. Struct.*, 2023, **1294**, 136385.

40 G. Kumar, K. Paul and V. Luxami, *New J. Chem.*, 2020, **44**, 12866–12874.

41 J. Zhao, H. Dong and Y. Zheng, *J. Phys. Chem. A*, 2018, **122**, 1200–1208.

42 Y. Zhao, Y. Yang, Y. Ma and Y. Li, *J. Lumin.*, 2018, **201**, 189–195.

43 M. J. Frisch, G. W. Trucks, H. B. Schlegel, G. E. Scuseria, M. A. Robb, J. R. Cheeseman, G. Scalmani, V. Barone, B. Mennucci, G. A. Petersson, H. Nakatsuji, M. Caricato, X. Li, H. P. Hratchian, A. F. Izmaylov, J. Bloino, G. Zheng, J. L. Sonnenberg, M. Hada, M. Ehara, K. Toyota, R. Fukuda, J. Hasegawa, M. Ishida, T. Nakajima, Y. Honda, O. Kitao, H. Nakai, T. Vreven, J. A. Montgomery Jr, J. E. Peralta, F. Ogliaro, M. Bearpark, J. J. Heyd, E. Brothers, K. N. Kudin, V. N. Staroverov, R. Kobayashi, J. Normand, K. Raghavachari, A. Rendell, J. C. Burant, S. S. Iyengar, J. Tomasi, M. Cossi, N. Rega, J. M. Millam, M. Klene, J. E. Knox, J. B. Cross, V. Bakken, C. Adamo, J. Jaramillo, R. Gomperts, R. E. Stratmann, O. Yazyev,

A. J. Austin, R. Cammi, C. Pomelli, J. W. Ochterski, R. L. Martin, K. Morokuma, V. G. Zakrzewski, G. A. Voth, P. Salvador, J. J. Dannenberg, S. Dapprich, A. D. Daniels, Ö. Farkas, J. B. Foresman, J. V. Ortiz, J. Cioslowski and D. J. Fox, *Gaussian 09*, Gaussian, Inc., Wallingford CT, 2009.

44 A. D. Becke, *J. Chem. Phys.*, 1993, **98**, 5648–5652.
45 C. Lee, W. Yang and R. G. Parr, *Phys. Rev. B: Condens. Matter Mater. Phys.*, 1988, **37**, 785–789.
46 J. T. R. Cammi, *J. Comput. Chem.*, 1995, **16**, 1449–1458.